Effects of Fabrication Materials and Methods on Flexible Resonant Sensor Signal Quality

Sadaf Charkhabi[a], Yee Jher Chan[a], Subhanwit Roy[b], Md Monirul Islam[a], Brock B. Duffield[a], Kyle J. Jackson[a], Lujia Bu[c], Sang-Hwan Kim[d], Andrew C. Hillier[a], Nathan M. Neihart[b], and Nigel F. Reuel[a]

[a]Department of Chemical and Biological Engineering, Iowa State University, Ames, IA, 50011

[b]Department of Electrical and Computer Engineering, Iowa State University, Ames, IA, 50011

[c]DuPont Electronics & Imaging-Emerging Technologies, Marlborough, MA, 01752

[d]DuPont Electronics & Imaging-Emerging Technologies, DuPont Experimental Station, Wilmington, DE 19803

*Corresponding Author - reuel@iastate.edu

Abstract

Inductor-capacitor (LC) resonant sensors can provide low-cost, contactless measurement in closed environments. In this work, three fabrication methods to produce flexible LC sensors are compared: screen-printed pastes, etched copper-coated polyimide, and wound metal wires. The LC sensors were interrogated by near-field coupled antennas driven by a vector network analyzer. The sensor response was analyzed by extracting the resonant frequency (MHz) and the peak-to-peak amplitude (dB) of the S_{21} scattering parameter. For screen-printed resonators, varying parameters such as print feature size (250 to 500 µm), conductive paste silver content (DuPont PE825 and 5028 for low and high silver content, respectively), curing condition (convection oven temperature and curing time), and paste viscosity (7.20 – 20.05 Pa·s) were explored. An empirical model was fit to this data to allow for prediction of required sensor line thickness needed to meet an application's required step-off distance. The screen-printed resonant sensors were then compared to copper-etched and wound metal wires to evaluate the cost and performance tradeoff of the three fabrication approaches. Finally, a use case of the flexible, screen-printed resonant sensors was demonstrated by contact-free measurement of fluid level of in a closed, curved container.

Keywords: Resonant sensor|Screen printing|LC sensor|Wireless |Radio frequency

Introduction

Flexible inductive-capacitive (LC) resonant sensors are an attractive, cost-effective solution to contact-free monitoring within closed systems. They have been used for measuring temperature[1–5], pressure[1,3–5], humidity[3–6], flow rate[7], chemical[8–11] and biological[12–15] parameters in industrial and medical applications.[3,16,17] LC sensors are interrogated by external antennas to measure changes in their scattering parameters via an interfaced vector network analyzer.[18] They have the added advantage of a passive architecture, with no on board power supply; instead, they are powered via near-field coupling with a vector network analyzer (VNA) and interrogation antennas.[19] Optimizing the quality of sensor design and materials is needed to achieve maximum step-off distance.

A few established, manufacturing approaches can be used for flexible LC sensors. First, copper-coated flexible substrates can be etched[7,10,15,20–22]; however, this method requires additional manufacturing steps for masking the pattern and handling etchant waste.[23,24] Second, screen printing LC sensors directly from conductive inks can be used for fast fabrication and can be directly printed on diverse substrates, such as silk[25], which would expand the use of LC sensors in wearable application. A third approach is patterning annealed wire, especially into fabrics to make RF devices.[26,27] These three methods all offer potential for LC sensor design but have yet been compared for their effectiveness in LC sensor performance.

This study demonstrates the effect of three fabrication methods on the signal quality of LC sensors: screen printing, etching, and wound metal wires of varying pure metals. For screen-printed sensors, screen feature size (250 to 500 µm), conductive paste silver content (DuPont PE825 and 5028 for low and high silver content, respectively), curing temperature, and substrate type (polyethylene terephthalate (PET) vs. polyimide (Kapton®)) are explored. Etched LC resonant sensors are made from copper coated polyimide (Pyralux®) and wound wire sensors are made from silver, gold, copper, and iron wires. The resonant frequency, peak-to-peak amplitude of S_{21} magnitude, and quality factor of the screen-printed sensors are evaluated. For sensor performance, the step-off distance and the sensitivity of frequency shift upon dielectric change were investigated and compared between the fabrication methods and materials. The

utility of an optimized, screen-printed LC sensor is then demonstrated by sensing the fluid level in a closed, curved vessel.

Results and Discussion

The Archimedean spiral resonators were designed and fabricated using three methods: 1) screen-printing conductive silver paste, 2) etching Pyralux® as described before[15], 3) and embedding wires in a laser-cut acrylic sheet (Figure 1). The initial part of this study is focused on screen printing the spiral inductor on flexible temperature tolerant PET (Melinex ST505) substrate using either low or high silver micro-flake conductive paste (DuPont PE825 and 5028 respectively). A screen containing varied trace line widths (250 to 500 µm in 50 µm intervals) was designed (Supplement 1). The sensor inner diameter, outer diameter, pitch, and overall trace length were all held constant (7 mm, 40 mm, 1.2 mm, and 1015.3 mm respectively). The pitch is defined as the conductive trace line width plus the spacing between lines; thus, as the line width increases, the spacing between conductive lines decreases. The curing conditions for the screen-printed samples were investigated (Supplement 2) and 110°C for 15 minutes was chosen as the curing condition for all the samples in this study. Other screen printing parameters such as the effect of silver content in the two pastes (low and high Ag paste) and silver paste viscosity (7.2 – 20.05 Pa·s) on the sensor performance were also studied (Supplement 3). In brief, lower viscosities resulted in smaller peak-to-peak amplitudes than higher viscosities and the resonant frequency was independent of the ink viscosity.

The sensor was interrogated by two coplanar antennas connected to a two-port VNA (Figure 2a). The antennas generate local electromagnetic fields when excited by the VNA. When the sensor is in close proximity with the antennas, coupling occurs and energy can be transferred to, and stored in, the sensor circuit. The energy is stored efficiently only at a narrow band of frequency, and the frequency where the most energy is stored is the resonant frequency, which is dependent on both the sensor geometry and the effective permittivity of the environment. The VNA measures the two-port scattering parameters (S-parameters) of the sensor. When measuring S_{11}, one reader antenna is used to measure reflected energy, and the resonance is identified by a trough in the magnitude of S_{11}. When evaluating S_{21}, a second reader antenna measures the energy transmitted through the coupled system. A symmetric

peak and trough in the magnitude of S_{21} are observed due to resonance; the sensor stores more energy from the excitation antenna near the trough frequency and the coupled, second measuring antenna receives more energy around the peak frequency.[28] We define the peak S_{21} frequency as the resonant frequency (aligns with the trough of S_{11}, see supplement 4) and monitor it as the sensor response in this work. Interrogating via S21 has a few advantages, namely 1) a non-symmetric response profile when used in co-planar mode that allows for position determination (and thus normalization of signal based on position[20]), 2) greater interrogation volume for an LC sensor, especially when placed on either side of the sensor[7], and 3) improved read range by tuning null mutual induction (the magnetic fluxes between the overlap area and non-overlap areas were equalized) at a specified frequency, such as a 40.68 MHz ISM band[29].

For both S_{11} and S_{21}, the resonant frequency is dependent on the effective permittivity of the surrounding and the sensor geometry, whereas the magnitude of S-parameters at the resonant frequency is dependent on the conductivity of the environment as well as the effective resistance of the sensor[10]. Changes in these signals are captured and recorded via the VNA with custom python scripts (Supplement 5). An example of signal shift when the sensor is exposed to air (control) and deionized water is shown in Figure 2b (solid lines). The shift in the peak resonant frequency (arrow in Figure 2b) is caused by changing the relative permittivity of sensor medium from $\varepsilon_{r,air} = 1$ to $\varepsilon_{r,water} = 80$.

We simulated the resonant sensor-reader system in Ansys HFSS to observe the electric field of the coupled system and confirm the out of plane sensitivity (Figure 2c). From simulation the electric field extends up to 2.6 cm and 1.8 cm in the Z direction (99% electric field magnitude) at the center and edge of the spiral resonator, respectively. The high electric field region indicates a higher sensitivity towards the surrounding permittivity. The experimental S_{21} signal is in fair agreement with the simulated results for the resonant sensor exposed to air (control) and deionized water (5 cm depth) above the resonator (dash lines in Figure 2b). The difference in frequency between the experimental and simulation results can be attributed to the slight difference in effective permittivity of the environment; whereas the difference in the magnitude of S_{21} can be attributed to the mixture of silver and organic blends (e.g. dibasic ester

solvent) in experiment and pure silver in simulation. Seeing these discrepancies between simulation and experiment, we further explored the effect of manufacturing method and material on the resonant sensor response. The sensor performance was quantified by measuring the 1) resonant frequency, 2) peak-to-peak amplitude, and 3) shift in resonant frequency upon change in dielectric (air to water), which are all depicted in the example sensor responses (Figure 2b and d); these values are extracted from the raw S_{21} magnitude data using custom MATLAB scripts (Supplement 6).

The width distribution of the screen-printed samples was analyzed using a digital microscope (Olympus DSX110) to correlate the manufactured screen width and measured print width (Supplement 7 and 8). This technique is useful to rapidly quantify the actual print dimensions as screen printing results can vary based on screen material, pressure, and printer used. A linear correlation between the measured print width and the screen width for high and low silver paste is shown in Eq. 1 ($R^2 = 0.97$) and Eq. 2 ($R^2 = 0.68$), respectively. Lower R-squared value obtained for the low silver was due to the higher deviation in 450 µm screen width samples.

$$High\ Ag: \quad Measured\ print\ width\ (\mu m) = 1.10 * Screen\ width\ (\mu m) + 47.4 \tag{1}$$

$$Low\ Ag: \quad Measured\ print\ width\ (\mu m) = 0.81 * Screen\ width\ (\mu m) + 200 \tag{2}$$

Screen widths below 250 µm were found to result in a higher failure rate with these commercial pastes (Supplement 9). The resolution of prints, though, is dependent on the properties of paste, substrate, and screen. For instance, Hyun et al. achieved a smaller feature, 22 µm print resolution using a fine-scale silicon stencil with 5 µm print features.[30] In another instance, Erath et al. reported the ability to further tune the resolution through substrate temperature.[31] Assessing the print variation from our screens across a single LC sensor, we observe a tight, normal distribution of width across the entire print length. Such uniformity is necessary to ensure that the calibration curve (spectral shift upon given change of target environmental variable or analyte) remains constant. Using a thickness gauge, the height of the screen-printed samples was determined to range between 7 to 15 µm, independent of the screen width.

For the screen-printed resonant sensors, we next measured the effect of silver content and screen line width on the sensor start frequency and peak to peak variability; the screen line width was incremented between 250 and 500 µm at 50 µm intervals; the low and high silver content pastes were used at a manufacturer-recommended viscosity of 10 Pa·s (Supplement 3). The resonant frequencies of the sensors remained within the small spectral window of 85.4 – 90.7 MHz regardless of the screen width of the inductor and paste type (Figure 3a); this is true except for the smaller screen widths of 250 and 300 µm. We hypothesize this larger variation is due to a larger number of defects and cracks in the lower resolution print which would cause a greater variation in start frequency based on our physical understanding of an LC sensor (*vide infra*). Additionally, we observe a larger dependence on peak-to-peak amplitude to screen width and silver content (Figure 3b), again observing greater variation in the smaller screen feature sizes.

We expect the resonant frequency to decrease with increasing screen width as the resonant frequency of the sensor is inversely related to the inductance and capacitance of the LC sensor (Eq. 3):[29]

$$f_{SR} = \frac{1}{2\pi\sqrt{LC}} \tag{3}$$

The width of the planar spiral inductors has a negligible effect on the inductance.[32] The self-capacitance, however, is expected to increase with increasing screen width, due to a decrease in the spacing between spiral lines, and subsequently decrease the resonant frequency. This trend was not observed for most of the screen widths since the height of the sensor is small; tightening the gap in between traces would have a smaller impact on the capacitance (Supplement 10). Using HFSS modeling, we observed a decrease in the resonant frequency (2.1 MHz) when changing the width from 0.2 mm to 0.6 mm (Supplement 11). This further confirms that the change in resonant frequency with changing screen width is small. These observations were also confirmed using empirical equations that predict the resonant frequency of Archimedean spirals (Supplement 12).[33] However, the peak-to-peak amplitude is impacted by the effective resistance within the sensor itself and the conductivity of the

surroundings. Increasing the screen width reduces the effective resistance and therefore increases the peak-to-peak amplitude (also observed from simulation). Moreover, higher silver content increases the conductivity of the silver paste, which again cause a decrement in the effective resistance and increases the peak-to-peak amplitude (Supplement 10). To investigate the flexibility of the sensors, the screen-printed and etched samples were bent and wrapped around an object of 1 cm diameter. Results showed that the signals remained relatively constant after unfolding (Supplement 13, low <100kHz level noise), with greater noise detected in the screen printed sensors vs. etched sensors. For a use case where bending occurs between measurements, the sensor response would need to be large (>1 MHz) to overcome this added system noise (see fluid level sensor in Figure 5 as an example of an LC sensor with large frequency response).

The screen printed LC sensors were also characterized by carefully measuring the 2-port scattering parameters using a custom coil characterization board that allows for direct coupling to the circuit (Supplement 14); the resistance and inductance values were then extracted for each sample using the one-port impedance parameter (Z_{11}) of a simple series resistor-inductor lumped model of the coil, at the minimum frequency of the VNA (300 kHz). For both high and low silver content samples, the resistance decreased as the screen width increased. As mentioned earlier, this result is reasonable since the resistance is inversely related with the cross-sectional area of the conductive line (Figure 3c). Moreover, the samples printed with high silver conductive paste demonstrate a lower resistance compared to the samples printed using low silver, regardless of the screen width, which is again due to the higher silver content of paste 5028. Notably, the quality factor (Q-factor) of an inductor in its operating angular frequency ($\omega = 2\pi f$) is defined as the ratio of reactance to resistance:

$$Q = \frac{\omega \, \mathrm{L}}{R} \tag{4}$$

In which L and R are the effective inductance and resistance of the coil, respectively. Therefore, the Q-factor for the screen-printed samples increased with the higher silver content and larger screen width (Figure 3d). A large Q-factor is a critical property of resonant sensors since it is

inversely proportional to bandwidth, and results in greater amplitudes at the resonant frequency as well as smaller bandwidth; this means the signal is easier to identify with an automated algorithm and can be more readily multiplexed with other sensors in different spectral windows. Resistance is inversely related to the spiral width (R ~ 1/A in which A is the cross-sectional area of the spiral inductor) and the Q-factor is directly proportional to the width of the spiral inductor (Q ~ 1/R based on Eq. 4). Thus, a function of form α/w and β·w is fit to the data for resistance (Eq. 5 for low Ag and Eq. 6 for high Ag) and Q-factor (Eq. 7 for low Ag and Eq. 8 for high Ag) respectively, with suitable coefficients of determination (R^2 = 0.97, 0.92, 0.86, 0.89 respectively). The 250 µm screen width was not included due to the line breaks in the printed resonator (Supplement 9).

$$R\ (\Omega) = 107000\left(\frac{1}{w\ (\mu m)}\right) \quad (5)$$

$$R\ (\Omega) = 50000\left(\frac{1}{w\ (\mu m)}\right) \quad (6)$$

$$Q_f = 4.2 \times 10^{-5} w\ (\mu m) \quad (7)$$

$$Q_f = 9.7 \times 10^{-5} w\ (\mu m) \quad (8)$$

Next, the effect of silver content and line width on sensor read range and sensitivity was evaluated; First, the peak-to-peak amplitude of the transmission coefficient is measured at 0 to 5 cm step-off distances (vertical distance between reader antenna and spiral inductor) with 0.5 cm intervals (Supplement 15). The larger the magnitude of peak-to-peak amplitude, the easier it is for an automated algorithm to find the resonant peak, especially when using a lower-cost portable VNA.[10,20] Higher silver content and larger line widths result in reduced spiral resistances and larger peak-to-peak amplitudes (Supplement 16). We fit this data to an empirical model to correlate the peak-to-peak amplitude of the forward transmission magnitude to the screen width of the spiral (w) and LC sensor-reader antenna step-off distance (d) for low (Eq. 9, R^2=0.92) and high (Eq. 10, R^2=0.89) silver content pastes. Using these equations with the screen width (w) to actual measured print width (p) transfer functions (Eqs. 1,2), the required width of the printed sensor for the low or high silver paste can be determined

based on the sensor's anticipated step-off distance in the given application and minimum detectable magnitude of the VNA (0.15 dB for the portable Copper Mountain VNA we use in this study, 0.5 dB for the lower cost MetroVNA used previously).[10,20] For instance, an LC sensor which is required to operate at 3 cm step-off distance from a reader antenna connected to a MetroVNA (with minimum detectable magnitude of 0.5 dB), should be designed to have a minimum print width of 426 μm and 51 μm for low and high silver paste, respectively.

$$low\ Ag: \quad Amp\ (dB) = (0.0394w\ (\mu m) + 0.394)\exp\ (-1.042d\ (cm)) \tag{9}$$

$$High\ Ag: \quad Amp\ (dB) = (0.0514w\ (\mu m) + 8.802)\exp\ (-0.962d\ (cm)) \tag{10}$$

Next, the shift in sensor resonant frequency in response to the addition of deionized water above the sensor (5 cm depth to fully saturate the signal) was measured and compared for varying print line widths of high and low silver pastes (Supplement 15). A control experiment was also run to confirm that this observed frequency shift occurred only due to a change in environment permittivity affecting the sensor and not the interrogation antennas (Supplement 17). It was observed that, in general, the silver content of the conductive paste or the screen width does not have a major effect on the frequency shift (Supplement 18). This can be explained via Eq. 3 in which the resonant frequency of the sensor is dependent on the capacitance and inductance. As mentioned above, neither the screen width nor the silver content has a major impact on the inductance of the LC sensor. Furthermore, the change in the capacitance is negligible since the effective permittivity of the environment (water, substrate, silver paste, etc.) is relatively consistent for all screen-printed samples (high silver 250 and 300 μm excluded). Therefore, the variations in the resonant frequency shift caused by changing the sensor feature width can be neglected.

The screen-printed resonant sensors were then compared to two other methods of manufacturing, copper-etched and wound pure metal wires, in order to bench-mark cost and performance tradeoff of these three techniques. First, the step-off distance test was conducted to measure the peak-to-peak amplitude in the range of 0 to 5 cm for each method (Figure 4a). It was observed that the etched resonant sensors have significantly higher peak-to-peak amplitude, followed by copper wire, silver wire, gold wire, cobalt wire, high silver screen-

printed, iron wire, and low silver screen-printed. As expected, the peak-to-peak amplitude has a direct relationship with the conductivity of the metal wire. Higher peak-to-peak amplitude in the etched samples than the copper metal wire can be explained by the larger trace cross-sectional area of the etched samples (0.018 mm^2) *vs.* the wire area (0.008 mm^2), resulting in a lower effective resistance. The peak-to-peak amplitude variation observed is therefore a combined effect from the materials and the cross-sectional area of the trace fabricated using different methods. It is also important to note that the peak-to-peak amplitude of the screen-printed samples are easily detectable (3-fold greater than noise threshold) up to a 2 cm reader-sensor distance. This signal threshold can be further reduced by improving the signal-to-noise ratio through impedance matching or further improvements in the reader; this study provides an estimate of relative detectable signal between different fabrication strategies.

Next, the resonant frequency shift caused by the addition of water was measured and the sensor response (Δ resonant frequency) was dependent on the fabrication method (etched, screen printed, and wound metal wire) (Figure 4a insert); however, there was not a significant difference observed in the resonant frequency shift when comparing different wound metal wires (copper: 7.61 (MHz), silver: 7.71 (MHz), gold: 7.47 (MHz), cobalt: 7.85 (MHz), iron: 7.80 (MHz)) or the screen-printed resonator fabricated with varying silver content paste (11.16 and 11.49 (MHz) for high and low silver, respectively), as discussed in Supplement 18. This observation can be attributed to two distinct cross-sectional profiles resulting from the three fabrication methods: circular cross-sections with curved edges from wound wires and flat rectangular profiles with planar edges from etched and printed; additionally, the three methods use different substrates (acrylic, PET, and polyimide). It appears that the planar edged geometry (screen printed and etched) have a greater susceptibility to permittivity change, resulting in a greater frequency shift for the same environmental change among these samples tested. Regarding the embedded metal wires, varying the type of material mainly changes the conductivity and effective resistance of the sensor, and therefore the peak-to-peak amplitude (which, again, has a direct impact on the distance at which the sensor can be interrogated). This is also confirmed by HFSS simulation, as shown in Figure 4b.

In addition to signal quality, there are multiple parameters that need to be taken into consideration to choose the best approach for fabrication of LC sensors such as material cost, fabrication time, achievable resolution, etc. These have been mapped for the eight candidate methods and materials used in this study (Table 1). Winding metal wire from pure, thin-diameter materials is a relatively expensive method of fabrication but could be reduced as less pure (especially copper) materials are used. Screen printing is the lowest cost method studied here, and could be further reduced with less expensive, copper-based pastes. However, copper paste cannot be thermally cured in a standard oven (due to oxidation) and therefore requires an alternative curing method such as photonic sintering.[34–37] Etching provides a good signal quality but is relatively more expensive in terms of fabrication time and cost compared to screen printing. One advantage of etching, however, is the ability to directly write a mask (using an XY-plotter) rather than waiting for a screen to be produced. The resolution of the etching method used in this study is mainly limited by the thickness of the mask drawn by the XY-plotter. Different patterning techniques can be used to obtain a better resolution, such as photolithography. However, this comes with added fabrication time and cost, and the resulting finer trace width can result in reduced signal quality due to increased resistance. Benefits of screen-printing include that it is well-suited for mass production and, as long as the peak-to-peak amplitude is beyond the acceptable threshold of its intended application, this fabrication method provides a significant economic advantage over the other methods.

To further illustrate the performance of these methods, we provide an illustrative example of screen-printed sensors in a real use case scenario. Three resonators are screen-printed (high silver paste and 400 µm screen width), on PET, thermally cured and affixed via transfer tape to the outside of a bottle to measure the fluid height in the vessel (Figure 5a). The length of the resonators was designed such that they each have distinct and detectable resonant frequencies (Figure 5b). A two-loop reader antenna connected to the VNA was placed in close proximity (1 cm step-off distance) of the sensors (Figure 5a). The resonant frequency shift of these sensors were measured for increasing (solid lines) and decreasing (dash lines) deionized water level up to 15 cm with 1.25 cm interval (Figure 5c). The resonant frequency drops with increasing water level since the local capacitance increases due to a change in the

effective permittivity of the sensor medium. This highlights how such sensors could be printed on packaging to measure changes in dielectric properties, such as increase in water content.

Conclusion

Resonant sensors were screen-printed using high and low silver content paste with screen widths ranging from 250 – 500 µm. The printed width of the samples has a linear relationship with the screen width for the high and low silver (Eq. 1 and 2). The relationship between screen width and the resistance and quality factor of sensor is shown in Eq. 5-8. The dependence of resonant frequency of the sensors on the screen feature width is considered negligible whereas the peak-to-peak amplitude has a linear relationship with the screen feature width due to the lower effective resistance of a larger trace width. On the signal quality perspective, a relationship was found for the magnitude of S_{21} in terms of screen feature width and step-off distance for low and high silver pastes (Eq. 9 and 10). The shift in resonant frequency, on the other hand, is independent of the screen width. The resonant frequency was independent of the viscosity (in the range of 7.20 – 20.05 Pa·s), whereas the peak-to-peak amplitude increases with increasing viscosity due to the higher content of conductive silver particles, giving better conduction. The screen-printing fabrication method was then compared to the etching and wound wire methods in terms of sensor quality and capability to mass produce. The response of the sensor's resonant frequency to the environment was found to be dependent on fabrication method whereas the peak-to-peak amplitude was dependent on the material's conductivity and the trace cross-sectional area that the fabrication method yields. In terms of mass production, screen-printing fabrication method provides a strong advantage in terms of material and time costs. Finally, an example application of the screen-printed sensors was demonstrated by sensing water level through a curved, plastic vessel.

Screen printing has the added advantage of directly printing the sensor on the substrate of interest conveniently and inexpensively. This could lead to many useful applications. For instance, resonant sensors could be printed directly on fabrics to monitor body fluids and temperature or they could be embedded directly into bandage materials. There is also room for further signal quality improvement by using new, screen-printable paste formulations with

reduced resistance and employing more advanced printing methods such as aligning multiple layers to increase the height of the sensor.

Figures and Tables

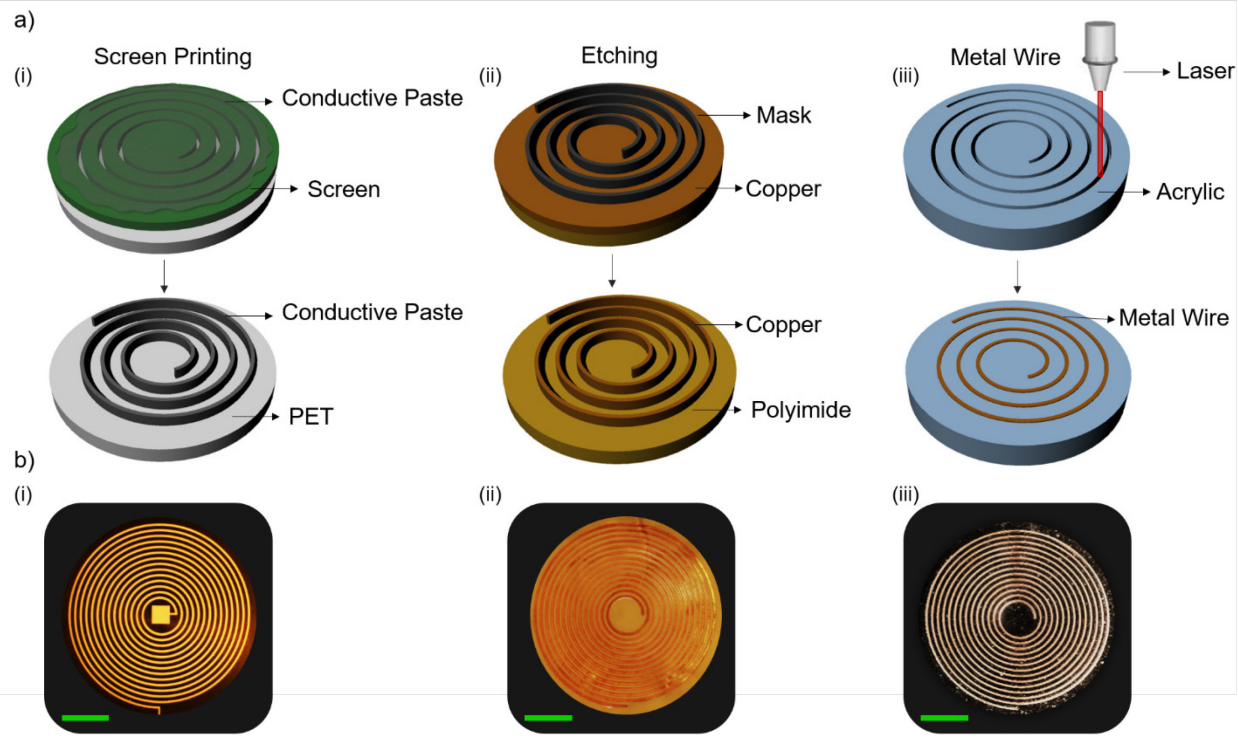

Figure 1. a) Schematic diagram of three fabrication processes for resonant sensors used in this work (i) screen printing, (ii) Pyralux® copper etching , and (iii) winding metal wire into laser-cut acrylic; b) Optical micrograph of (i) screen-printed resonant sensor, (ii) etched, and (iii) metal-wire; (scale bar = 10 mm).

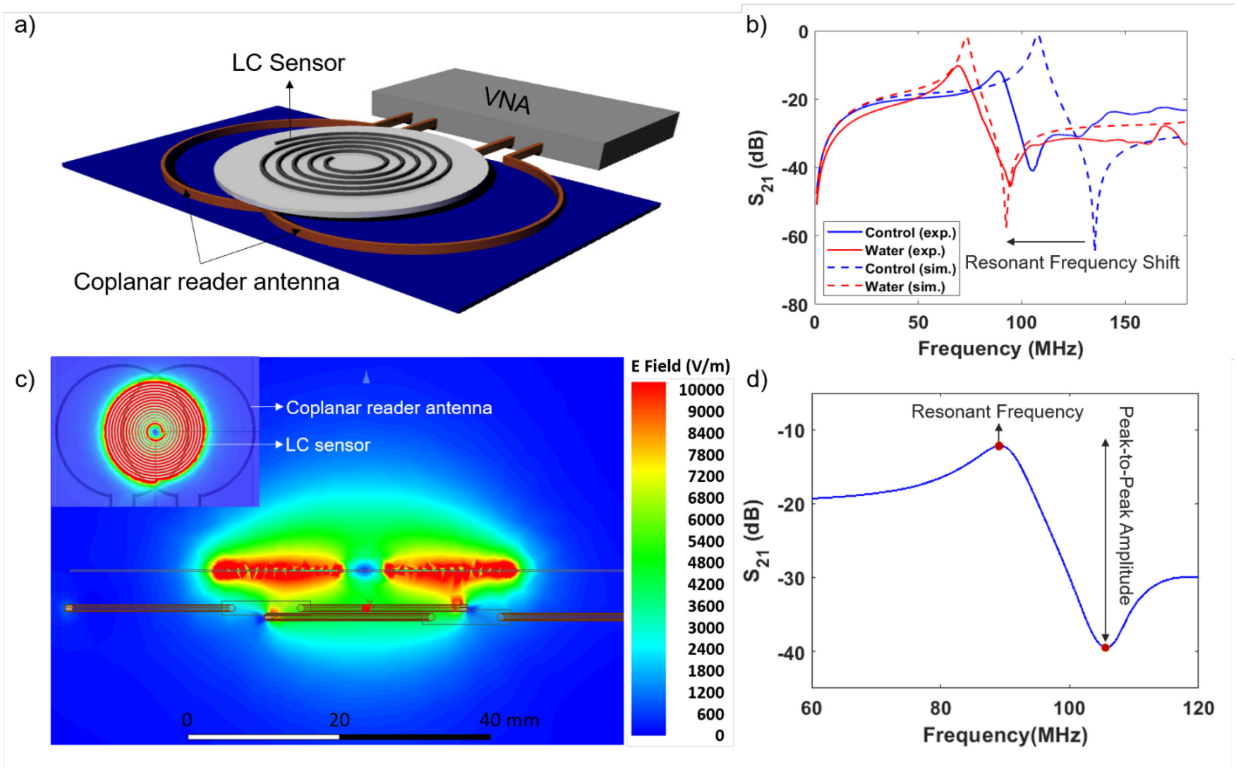

Figure 2. a) Schematic of the resonant sensor system consisting of an open-circuit Archimedean spiral LC sensor and an external reading antenna connected to a vector network analyzer (VNA); b) Simulated and experimental sensor response when exposed to air and DI water (the arrow shows the shift in the resonant frequency upon change in the local permittivity); c) Side view of the electric field simulation of the sensor energized by VNA depicting regions of maximum coupling or power transmission (insert graph is the top view of sensor on the two loop reader antenna); d) Example empirical data of an LC sensor transmission magnitude response with resonant frequency and peak-to-peak amplitude annotated.

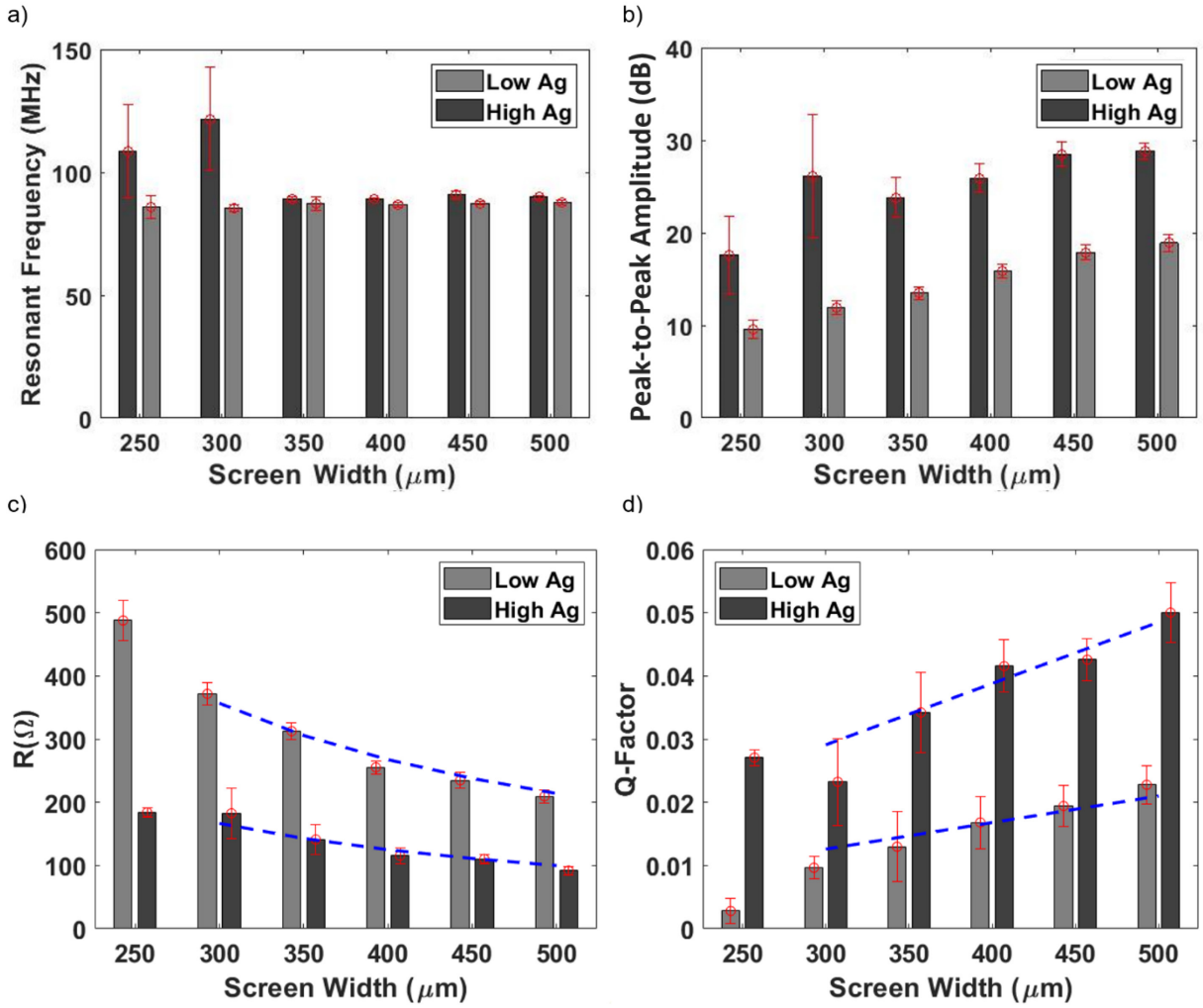

Figure 3. Effect of the conductive paste silver content and screen width on a) resonant frequency and b) peak-to-peak amplitude for n>17 samples per paste and width. Coil characterization board was used to measure 2-port S-parameters on VNA in order to measure the c) R and; d) Q-factor of resonant sensors. The dash lines are the empirical fits (Eq. 5-8).

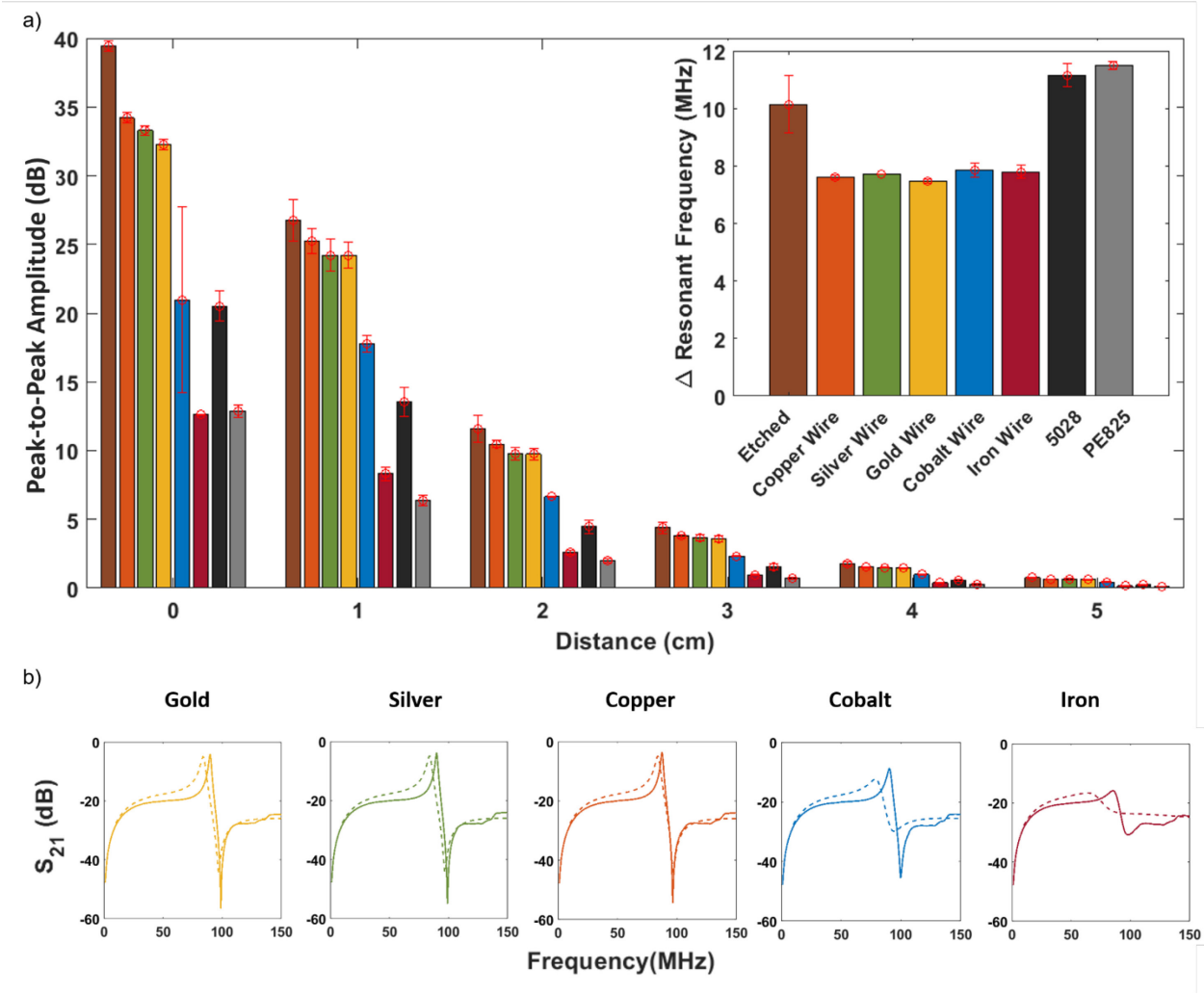

Figure 4. a) Comparison of different fabrication methods of resonant sensors in response to vertical distance between the spiral inductor and reading antenna. The insert demonstrates the sensor response to 5 cm DI water above the sensor; b) simulated and experimental transmission loss signals for varying metal wires.

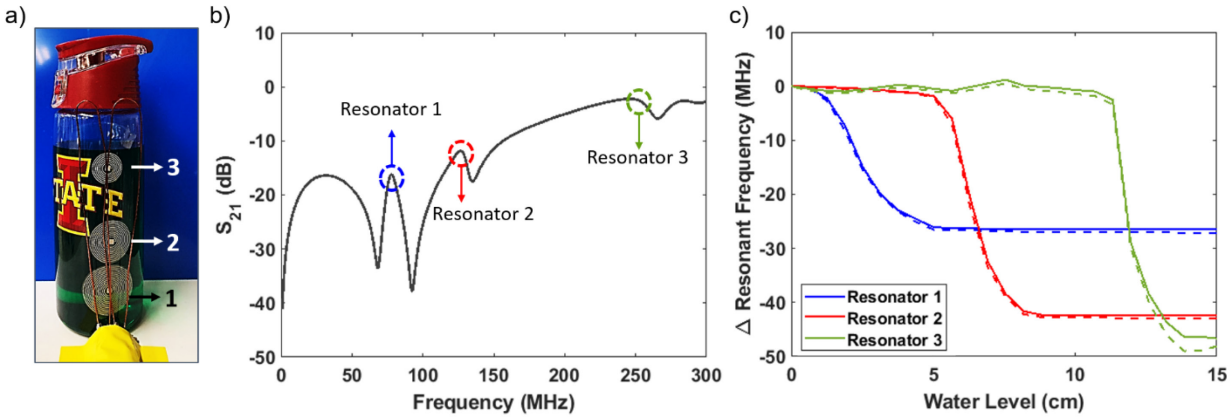

Figure 5. Wireless detection of water level using screen-printed resonant sensors. a) setup of the sensing system showing three resonators and two-loop reader antenna; b) example of S_{21} sensor response showing initial self-resonant frequencies of the resonators (water level = 0 cm); c) shift in the resonant frequency of the sensors due to change in the fluid level inside the water bottle.

Table 1. Comparison of different fabrication methods of resonant sensors in terms of material cost, fabrication time, and minimum feature size, and maximum sensor-reader step-off distance.

Method	Material cost ($)/unit)	Fabrication time (min/unit)	Approximate resolution (µm)	Maximum step-off (cm)
Copper Etching	2.96	30	400	4
Copper Wire	0.25	30	100	4
Silver Wire	19.25	30	100	4
Gold Wire	41.95	30	100	4
Cobalt Wire	71.75	30	100	4
Iron Wire	18.05	30	100	3
Screen Printing (High Ag)	0.4	0.6	300	3
Screen Printing (Low Ag)	0.3	0.6	300	2

Acknowledgment

Funding for this research was provided in part by an NSF Industrial Innovation and Partnerships PFI-RP grant under award #1827578 and Iowa State University startup funds. The authors also thank DuPont for capital equipment donations.

Supporting Information

The supporting information associated with this article is available free of charge at doi:

References

(1) Nabipoor, M.; Majlis, B. Y. A New Passive Telemetry LC Pressure and Temperature Sensor Optimized for TPMS. *J. Phys. Conf. Ser.* **2006**, *34* (1), 770–775. https://doi.org/10.1088/1742-6596/34/1/127.

(2) Amin, E. M.; Karmakar, N. Development of a Chipless RFID Temperature Sensor Using Cascaded Spiral Resonators. *2011 IEEE SENSORS Proc.* **2011**, 554–557. https://doi.org/10.1109/ICSENS.2011.6127344.

(3) Huang, Q. A.; Dong, L.; Wang, L. F. *LC Passive Wireless Sensors Toward a Wireless Sensing Platform: Status, Prospects, and Challenges*; 2016; Vol. 25, pp 822–841. https://doi.org/10.1109/JMEMS.2016.2602298.

(4) Li, C.; Tan, Q.; Jia, P.; Zhang, W.; Liu, J.; Xue, C.; Xiong, J. Review of Research Status and Development Trends of Wireless Passive Lc Resonant Sensors for Harsh Environments. *Sensors (Switzerland)* **2015**, *15* (6), 13097–13109. https://doi.org/10.3390/s150613097.

(5) Ong, K. G.; Grimes, C. A.; Robbins, C. L.; Singh, R. S. Design and Application of a Wireless, Passive, Resonant-Circuit Environmental Monitoring Sensor. *Sensors Actuators, A Phys.* **2001**, *93* (1), 33–43. https://doi.org/10.1016/S0924-4247(01)00624-0.

(6) Harpster, T. J.; Stark, B.; Najafi, K. A Passive Wireless Integrated Humidity Sensor. *Sensors Actuators A Phys.* **2002**, *95* (2–3), 100–107.

(7) Charkhabi, S.; Chan, Y. J.; Hwang, D. G.; Frey, S. T.; Bartlett, M. D.; Reuel, N. F. Kirigami-

Enabled, Passive Resonant Sensors for Wireless Deformation Monitoring. *Adv. Mater. Technol.* **2019**, *4* (5), 1–8. https://doi.org/10.1002/admt.201800683.

(8) Potyrailo, R. A.; Morris, W. G. Multianalyte Chemical Identification and Quantitation Using a Single Radio Frequency Identification Sensor Identification and Quantitation Using a Single Conventional. **2007**, *79* (1), 45–51. https://doi.org/10.1021/ac061748o.

(9) Lei, M.; Baldi, A.; Pan, T.; Gu, Y.; Siegel, R. A.; Ziaie, B. A Hydrogel-Based Wireless Chemical Sensor. In *17th IEEE International Conference on Micro Electro Mechanical Systems. Maastricht MEMS 2004 Technical Digest*; IEEE, 2004; pp 391–394.

(10) Carr, A. R.; Patel, Y. H.; Neff, C. R.; Charkhabi, S.; Kallmyer, N. E.; Angus, H. F.; Reuel, N. F. Sweat Monitoring beneath Garments Using Passive, Wireless Resonant Sensors Interfaced with Laser-Ablated Microfluidics. *npj Digit. Med.* **2020**, *3* (1), 1–9.

(11) Charkhabi, S.; Carr, A. R.; Wu, J.; Roy, S.; Beierle, A. M.; Thomas, D. K.; Neihart, N. M.; Reuel, N. F. Resonant Sensor Arrays for Wireless Characterization of Solvated Ions. *ChemRxiv* **2019**.

(12) Potyrailo, R. A.; Nagraj, N.; Tang, Z.; Mondello, F. J.; Surman, C.; Morris, W. Battery-Free Radio Frequency Identi Fi Cation (RFID) Sensors for Food Quality and Safety. **2012**. https://doi.org/10.1021/jf302416y.

(13) Ong, K. G.; Bitler, J. S.; Grimes, C. A.; Puckett, L. G.; Bachas, L. G. Remote Query Resonant-Circuit Sensors for Monitoring of Bacteria Growth: Application to Food Quality Control. *Sensors* **2002**, *2* (6), 219–232.

(14) Tan, E. L.; Ng, W. N.; Shao, R.; Pereles, B. D.; Ong, K. G. A Wireless, Passive Sensor for Quantifying Packaged Food Quality. *Sensors* **2007**, *7* (9), 1747–1756. https://doi.org/10.3390/s7091747.

(15) Charkhabi, S.; Beierle, A.; McDaniel, M. D.; Reuel, N. F. Resonant Sensors for Low-Cost, Contact-Free Measurement of Hydrolytic Enzyme Activity in Closed Systems. *ACS Sensors* **2018**. https://doi.org/10.1021/acssensors.8b00267.

(16) Andringa, M. M.; Neikirk, D. P.; Dickerson, N. P.; Wood, S. L. Unpowered Wireless Corrosion Sensor for Steel Reinforced Concrete. In *SENSORS, 2005 IEEE*; IEEE, 2005; pp 4-pp.

(17) Chen, P.-J.; Rodger, D. C.; Saati, S.; Humayun, M. S.; Tai, Y.-C. Microfabricated Implantable Parylene-Based Wireless Passive Intraocular Pressure Sensors. *J. Microelectromechanical Syst.* **2008**, *17* (6), 1342–1351.

(18) Charkhabi, S. Resonant Sensors for Passive, Real-Time, and Wireless Characterization of Biological Analytes. **2018**.

(19) Elsherbiny, O.; Roy, S.; Charkhabi, S.; Carr, A. R.; Beierle, A. M.; Reuel, N. F.; Neihart, N. M. Physically Inspired Circuit Model for Systematic Analysis of Resonant Ion Sensor.

(20) Chan, Y. J.; Carr, A. R.; Charkhabi, S.; Furnish, M.; Beierle, A. M.; Reuel, N. F. Wireless Position Sensing and Normalization of Embedded Resonant Sensors Using a Resonator Array. *Sensors Actuators, A Phys.* **2020**, *303*, 111853. https://doi.org/10.1016/j.sna.2020.111853.

(21) Crum, B.; Li, W. Parylene-Based Fold-and-Bond Wireless Pressure Sensor. In *The 8th Annual IEEE International Conference on Nano/Micro Engineered and Molecular Systems*; IEEE, 2013; pp 1155–1158.

(22) Chen, G.-Z.; Chan, I.-S.; Leung, L. K. K.; Lam, D. C. C. Soft Wearable Contact Lens Sensor for Continuous Intraocular Pressure Monitoring. *Med. Eng. Phys.* **2014**, *36* (9), 1134–1139.

(23) Blunn, A. J.; Treasure, D. M. Process and Apparatus for Generating or Recovering Hydrochloric Acid from Metal Salt Solutions. Google Patents March 2019.

(24) Hiorns, R. C.; Moliton, A. *Optoelectronics of Molecules and Polymers*; Springer Series in Optical Sciences; Springer New York, 2010.

(25) Voutilainen, J.-V.; Happonen, T.; Häkkinen, J.; Fabritius, T. All Silk-Screen Printed Polymer-Based Remotely Readable Temperature Sensor. *IEEE Sens. J.* **2014**, *15* (2), 723–

733.

(26) Stoppa, M.; Chiolerio, A. Wearable Electronics and Smart Textiles: A Critical Review. *sensors* **2014**, *14* (7), 11957–11992.

(27) Dion, G.; Dandekar, K. R.; Gogotsi, Y.; Patron, D.; Jost, K. A.; Le, M. N.; Fisher, J. W.; Watt, S. J.; Cook, A. C. Wearable Power Harvesting System. Google Patents May 2018.

(28) Harder, M.; Hu, C.-M. Cavity Spintronics: An Early Review of Recent Progress in the Study of Magnon–Photon Level Repulsion. In *Solid State Physics*; Elsevier, 2018; Vol. 69, pp 47–121.

(29) Reuel, N. F.; McAuliffe, J. C.; Becht, G. A.; Mehdizadeh, M.; Munos, J. W.; Wang, R.; Delaney, W. J. Hydrolytic Enzymes as (Bio)-Logic for Wireless and Chipless Biosensors. *ACS Sensors* **2016**, *1* (4), 348–353. https://doi.org/10.1021/acssensors.5b00259.

(30) Hyun, W. J.; Lim, S.; Ahn, B. Y.; Lewis, J. A.; Frisbie, C. D.; Francis, L. F. Screen Printing of Highly Loaded Silver Inks on Plastic Substrates Using Silicon Stencils. *ACS Appl. Mater. Interfaces* **2015**, *7* (23), 12619–12624.

(31) Erath, D.; Filipović, A.; Retzlaff, M.; Goetz, A. K.; Clement, F.; Biro, D.; Preu, R. Advanced Screen Printing Technique for High Definition Front Side Metallization of Crystalline Silicon Solar Cells. *Sol. energy Mater. Sol. cells* **2010**, *94* (1), 57–61.

(32) Mohan, S. S.; Hershenson, M.; Boyd, S. P.; Lee, T. H. Simple Accurate Expressions for Planar Spiral Inductances. **1999**, *34* (10), 1419–1424.

(33) Hooker, J. W.; Ramaswamy, V.; Member, S.; Arora, R. K.; Member, L. S.; Edison, A. S.; Withers, R. S.; Nast, R. E.; Brey, W. W.; Application, A. An Empirical Expression to Predict the Resonant Frequencies of Archimedean Spirals. **2015**, *63* (7), 2107–2114.

(34) Schroder, K.; McCool, S.; Furlan, W. Broadcast Photonic Curing of Metallic Nanoparticle Films. *NSTI Nanotech May* **2006**, *7*, 11.

(35) Perelaer, J.; Abbel, R.; Wünscher, S.; Jani, R.; Van Lammeren, T.; Schubert, U. S. Roll-to-roll Compatible Sintering of Inkjet Printed Features by Photonic and Microwave

Exposure: From Non-conductive Ink to 40% Bulk Silver Conductivity in Less than 15 Seconds. *Adv. Mater.* **2012**, *24* (19), 2620–2625.

(36) Akhavan, V.; Schroder, K.; Pope, D.; Rawson, I.; Edd, A.; Farnsworth, S. Reacting Thick-Film Copper Conductive Inks with Photonic Curing. In *Proceedings of the 13th International Symposium on Electronics Packaging (ICEP2013). The Japan Institute of Electronics Packaging (JIEP)*; 2013.

(37) Rosen, Y. S.; Yakushenko, A.; Offenhäusser, A.; Magdassi, S. Self-Reducing Copper Precursor Inks and Photonic Additive Yield Conductive Patterns under Intense Pulsed Light. *ACS omega* **2017**, *2* (2), 573–581.